

Kalib: Markerless Hand-Eye Calibration with Keypoint Tracking

Tutian Tang^{1*}, Minghao Liu^{1*}, Wenqiang Xu¹ and Cewu Lu¹

Abstract—Hand-eye calibration involves estimating the transformation between the camera and the robot. Traditional methods rely on fiducial markers, involving much manual labor and careful setup. Recent advancements in deep learning offer markerless techniques, but they present challenges, including the need for retraining networks for each robot, the requirement of accurate mesh models for data generation, and the need to address the sim-to-real gap. In this letter, we propose Kalib, an automatic and universal markerless hand-eye calibration pipeline that leverages the generalizability of visual foundation models to eliminate these barriers. In each calibration process, Kalib uses keypoint tracking and proprioceptive sensors to estimate the transformation between a robot’s coordinate space and its corresponding points in camera space. Our method does not require training new networks or access to mesh models. Through evaluations in simulation environments and the real-world dataset DROID, Kalib demonstrates superior accuracy compared to recent baseline methods. This approach provides an effective and flexible calibration process for various robot systems by simplifying setup and removing dependency on precise physical markers. The code, data, and supplementary materials are available at <https://sites.google.com/view/hand-eye-kalib>.

I. INTRODUCTION

Hand-eye calibration, which is to estimate the transformation between the camera and the robot, is one of the fundamental problems for robot manipulation with a long history [1]–[4]. A precise and easy-to-use hand-eye calibration method not only facilitates the successful interaction of robots with the environment but also enables researchers to rapidly iterate the setups and downstream algorithms in laboratories.

Traditional methods usually rely on calibration boards with certain patterns, such as AprilTag [5] and ArUco [6] markers. These markers should be printed with precise dimensions, affixed flatly on a rigid board, and carefully mounted. The whole process is tedious even for experienced users. Recently, with the development of deep learning, markerless techniques have drawn increasing attention due to the potential to eliminate the need for the calibration board [7]–[10]. However, there are three drawbacks to current deep learning models. (1) Generalizability. We need to train the neural networks for each new robot since the networks trained on specific data usually do not generalize well to different embodiments. (2) Adaptability. In order to

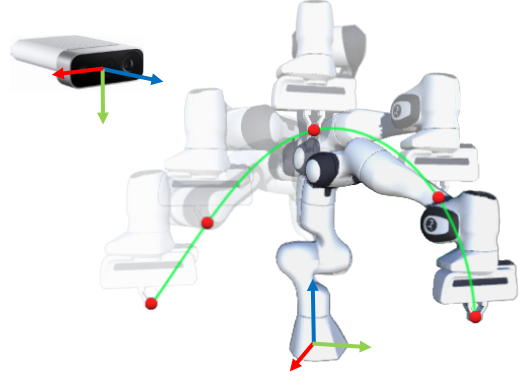


Fig. 1. The proposed method solves the hand-eye calibration problem by tracking the position of a predefined reference point with the existing visual foundation models.

generate high-quality training data, we need to know the robot’s accurate mesh model, which may not be available due to commercial reasons or users’ modifications, such as electronic skin and extra sensors. (3) Sim-to-real gap. We have to carefully solve it to make the network trained on synthetic data work in the real world.

But do we have to go through these time-consuming procedures? Not necessarily. After all, what we essentially require is the coordinate transformation relationship between certain points on the robot and their corresponding points in the camera space. The first part is easy to acquire since we can calculate the coordinates of any reference point in the robot space with forward kinematics. Then, the problem left is whether we can track the position of the point on the image frame accurately. We note that the recent visual foundation models [12]–[14] demonstrate excellent generalizability and zero-shot accuracy on real-world images, which can spare us the trouble of generating data and training models. With these considerations in mind, we present **Kalib**, a universal, automatic, markerless hand-eye calibration pipeline. In each calibration process, we define a reference point on the robot and make it move in the workspace. With the off-the-shelf foundation model for keypoint tracking and the proprioceptive sensors integrated into the robot, we acquire both the 2D coordinate on the image frame and its 3D coordinate in the robot space. Finally, a Perspective-n-Point (PnP) solver estimates the camera-to-robot transformation. The proposed method can work with common robot arms and grippers without training any networks, therefore eliminating the need for the robot’s exact mesh model.

Our main contribution is the **Kalib** method for markerless hand-eye calibration. To evaluate our method, we first test

*Equal contribution.

¹{tttang, lmh209, vinjohn, lucewu}@sjtu.edu.cn. Tutian Tang, Minghao Liu and Wenqiang Xu are with School of Electronic Information and Electrical Engineering, Shanghai Jiao Tong University, Shanghai, China. Cewu Lu is the corresponding author, a member of Qing Yuan Research Institute and MoE Key Lab of Artificial Intelligence, AI Institute, Shanghai Jiao Tong University, Shanghai, China.

TABLE I
COMPARISON WITH EXISTING METHODS.

Category	Type	Markerless	Setting	Required Prior	No-Training	Occlusion	Workload
Traditional	Board [4]	✗	Both	Kinematics	✓	/	Heavy
	SfM [11]	✓	Eye-in-Hand	Kinematics	✓	/	Low
Learning-Based	Keypoint [7]	✓	Eye-on-Base	+ Mesh Model	✗	/	Low
	Mask [9]	✓	Eye-on-Base	+ Mesh Model	✗	✗	Medium
	6D Pose [10]	✓	Eye-on-Base	+ Mesh Model	✗	/	Low
	Ours	✓	Both	Kinematics	✓	✓	Low

For each type, we select one representative method for comparison. **Markerless:** We mark ✓ if no fiducial marker is required. **Setting:** Whether the method can work under eye-in-hand or eye-on-base setting, or both. **Required Prior:** Kinematics means the kinematic model is the only required prior. Mesh model means the precise mesh model is also required. **No-Training:** We mark ✓ if there is no need to re-train neural networks on a new setup. **Occlusion:** Whether the method can work under occlusion. / means not applicable or not reported. **Workload** compares the relative amount of manual work. **Bold items** are considered superior to others.

its accuracy in a simulation environment built with RFUniverse [15]. Results show the translational and rotational error is around 0.3 cm and 0.4 degrees, respectively, on average, outperforming the recent baseline method EasyHeC [9] and is on-par with the marker-based traditional method. We also conduct extensive experiments on DROID [16], a large-scale real-world dataset for robot manipulation. Results show that our method outperforms the baseline method, and its markerless nature enables it to serve as a remedial measure when the traditional methods used for building the dataset produce results with significant errors.

II. RELATED WORK

A. Hand-Eye Calibration

Hand-eye calibration has been studied for a long time. There are roughly two different settings of hand-eye calibration, namely, *eye-on-base* and *eye-in-hand*. Traditional methods [1], [2], [4], [17], [18] rely on calibration boards with fiducial markers [5], [6], [19] or canonical objects [20]. These markers should be printed, glued, and mounted with care. Not only does the whole process involve much manual labor, but there are also many detailed factors that can lead to inaccurate marker detection and finally result in the failure of calibration, for example, motion blur, extreme lighting conditions, improper size, and unexpected movement of markers [3]. Therefore, in order to save manual labor, the need for markerless calibration methods lasts for long. The pioneers [11], [21], [22] adopt Structure-from-Motion (SfM) techniques to estimate the camera motion during the calibration process, which only work under the eye-in-hand setting.

Later, with the advancement of deep learning, many works utilize neural networks to calibrate the camera, especially under the eye-on-base setting. For example, DREAM [7] and CtRNet [8] adopt the keypoints estimation networks to detect the 2D keypoints of the robot and use the PnP algorithm to estimate the camera pose. The idea behind this is that the robot itself is a standardized item with rich visual features, so it can act as the marker for calibration. Other works adopt 6D pose estimation networks [10], [23] to directly estimate the transformation of the robot arm in the camera coordinate. However, the direct 6D pose estimation is

reported to be noisy and sensitive to many factors, including light conditions, occlusion, and the sim-to-real gap [24]. To ease this problem, a more recent work, EasyHeC [9], first estimates the 6D pose and further refines it through the mask prediction and differentiable rendering mechanism, which requires the precise mesh model. All these methods involve training networks for specific robots. The trained networks can not generalize to new robots, so users have to retrain them on a new setup. In comparison, the proposed **Kalib** adopts existing visual foundation models to prevent the users from training any networks and eliminate the need for the precise mesh model. Moreover, **Kalib** can solve both eye-in-hand and eye-on-base settings, even under self-occlusion, making it especially suitable for today’s research community where egocentric cameras are popular [16]. We summarize the comparison in Table I.

B. Keypoint Tracking with Foundation Models

Keypoint tracking is to recover the motion of certain pixels in videos. Early studies formulate it as an optical flow estimation problem [25], [26] or particle tracking problem [27], [28]. However, these methods focus on low-level image features and thus lack the ability for long-term tracking. Recent advancement in visual foundation models enables the encoder networks to extract rich low-level and instance-level features, making it possible to track any pixels in image sequences [29], [30]. Co-Tracker [14] can jointly track the pixels representing the same instance to improve accuracy and robustness. SpatialTracker [31] lifts the 2D pixels into the 3D space, making it robust under heavy occlusion and complex movement, and therefore, we utilize it to track the 2D keypoints of the robot in this work.

III. METHOD

A. Overview

Given the robot kinematics and the intrinsic camera parameters, the hand-eye calibration is to estimate the transformation X between the camera system A and the robot system B which satisfies $AX = XB$ [2]. In this letter, the camera intrinsic parameters are represented as the intrinsic matrix $\mathbf{K}_{3 \times 3}$ and the transformation X is represented as a 4×4 matrix $\mathbf{T} \in SE(3)$. To break it down further,

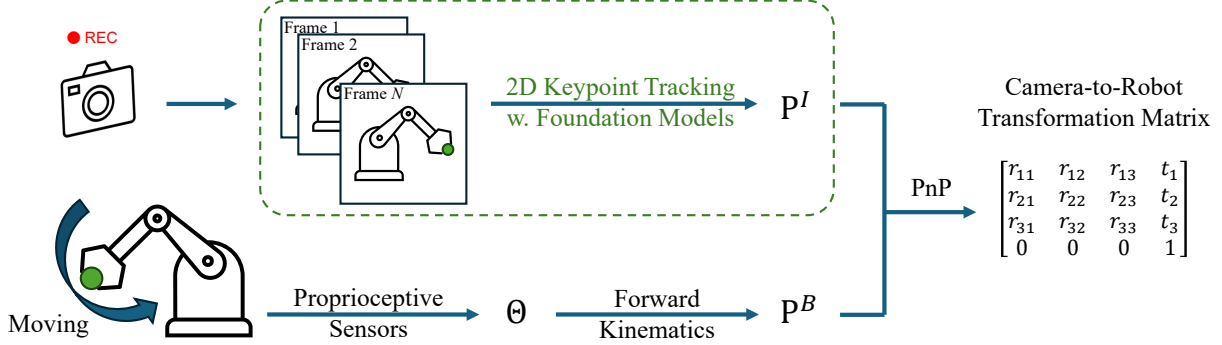


Fig. 2. Given N consecutive camera frames, we first track the reference point on the image plane with foundation models (Sec. III-B). At the same time, the joint positions of the robot are recorded by proprioceptive sensors. The coordinate of the reference point in the robot base coordinate can be derived by forward kinematics (Sec. III-C). Finally, the PnP module can estimate the camera-to-robot transformation matrix.

depending on the scenario, the camera is mounted either with a fixed transformation to the robot base \mathbf{T}^{CB} in the eye-on-base setup or with a fixed transformation to the end-effector \mathbf{T}^{CE} in the eye-in-hand setup. Note that these two settings are fundamentally dual, as the transformation between the base and end-effector \mathbf{T}^{BE} can be derived with forward kinematics and it always holds $\mathbf{T}^{CE} = \mathbf{T}^{CB}\mathbf{T}^{BE}$ at each frame. Therefore, we will first discuss the details of the proposed method under the eye-on-base setting, and finally demonstrate how it may operate under the eye-in-hand setup with minimal modifications in Section III-D.

Figure 2 shows the pipeline of the proposed method. Given N consecutive frames that record the movement of the robot, we first select a reference point on the robot as the keypoint and track its 2D position on each image $P_i^I(u_i, v_i), i = 1, 2, \dots, N$ (Sec. III-B). Simultaneously, we can record the joint positions of the robot θ_i at each frame with the proprioceptive sensors integrated into the robot. The 3D coordinate of the reference point in the robot base coordinates $P_i^B(x_i, y_i, z_i)$ can therefore be derived by forward kinematics. Finally, the PnP module will estimate the camera-to-robot transformation matrix \mathbf{T}^{CB} (Sec. III-C).

B. 2D Keypoint Tracking

a) *Tracking Target:* Before the tracking process begins, we need to decide the target to track. A potential candidate should meet the following three conditions. First, it should be one of the joints in the kinematic model of the robot so that we can precisely determine its 3D coordinate in the robot coordinate with the proprioceptive sensors. Second, it should be generally unobstructed in the camera view during the robot’s movement. Third, it should correspond to clear visual features on the robot’s surface so that the tracking module can work precisely. Most joint keypoints of popular robot arms do not satisfy the aforementioned third condition. More specifically, the joints are located internally in the robot, and therefore, their projected points onto the surface of the robot vary under different camera perspectives. This inconsistency between the external features and the internal keypoints may confuse the neural networks. Among these joints, which are mostly unsuitable, the tool center point

(TCP) is an exception. On typical parallel grippers, the TCP is often defined as the tips of the fingers when they are closed. It satisfies the three conditions, so we decided to use it as the tracking target in our method.

b) *TCP Tracking:* We can use visual foundation models to track the TCP on the 2D images. Given N camera frames and the initial position of TCP $P_1^I(u_1, v_1)$, the tracking module will give the 2D positions of the target on each image frame $\mathbf{P}^I = \{(u_i, v_i) | i = 1, 2, \dots, N\}$. We use SpatialTracker [31] as the tracking module because it achieves a good balance between accuracy and inference speed. To note, the off-the-shelf foundation models already demonstrate excellent generalizability and zero-shot accuracy, so we do **not** retrain or finetune it on any dataset. This is exactly the application scenario we want. The initial position of TCP on the first frame can be annotated by a single mouse click, which is much easier than annotating the mask or 6D pose in previous methods. Moreover, if the camera and robot’s poses do not dramatically change compared with the previous calibration, we can reuse the previous annotation.

C. Camera Pose Estimation

In each calibration process, the joint positions of the robot at each frame are also recorded $\Theta = \{(j_{i1}, j_{i2}, \dots, j_{iJ}) | i = 1, 2, \dots, N\}$, where N is the number of recorded frames, and J is the number of controllable joints on the robot. We can then use forward kinematics [32] to compute the 3D coordinates of the reference point $\mathbf{P}^B = \{(x_i, y_i, z_i) | i = 1, 2, \dots, N\}$ in the robot base coordinate.

Based on the camera model, the 2D pixel $P^I(u_i, v_i)$ on the image frame and the corresponding 3D coordinate in the robot root coordinate $P^B(x_i, y_i, z_i)$ obey the following equation:

$$s \cdot \hat{P}^I = \begin{bmatrix} \mathbf{K}_{3 \times 3} & \mathbf{0}_{3 \times 1} \\ \mathbf{0}_{1 \times 3} & 1 \end{bmatrix}_{4 \times 4} \cdot \mathbf{T}^{CB} \cdot \hat{P}^B,$$

where s is a scaling factor, and \hat{P} denotes the homogeneous representation of P .

Now, we can formulate the camera pose, \mathbf{T}^{CB} , estimation as a Perspective-n-Point (PnP) problem. Given \mathbf{K} , \mathbf{P}^I and \mathbf{P}^B , a PnP solver can solve \mathbf{T}^{CB} . A minimum of three

corresponding points are required [33]. We will show that increasing number of points (which equals the number of frames in our setting) can lead to better precision in Section IV-D.1. In practice, since common cameras operate at 30 FPS, the robot movement lasting 10 to 20 seconds can easily generate hundreds of corresponding points. In addition, to avoid some known limitations of PnP, we should avoid the keypoints being collinear or coplanar [6]. In other words, the TCP should traverse the entire 3D workspace under the camera’s view as much as possible instead of being confined to a single plane or a line. Robot arms with 6 or 7 degrees of freedom (DoF) can easily achieve this. In terms of implementation, we adopt the Efficient PnP (EPnP) solver [34] with the RANSAC scheme [35] implemented in OpenCV [36], in order to minimize the impact of noise and potential outliers generated during the keypoint tracking process.

D. Eye-in-Hand Setup

In previous sections, we discussed the details of our method in the eye-on-base setting. In this section, we will show how our method can work under the eye-in-hand setup with minimal modifications. Recap that in this setting, the camera is mounted with a fixed transformation to the end-effector, denoted as \mathbf{T}^{CE} , and our goal is exactly to estimate it. We select the intersection point of the shell of the robot base and the x axis of the robot coordinate (which is usually interpreted as the *forward* direction of the robot) as the reference point to track. This point meets the three conditions aforementioned in Section III-B, and its coordinate in the robot base $P_{ref}^B(x_{ref}, 0, 0)$ can be easily measured. During the calibration process, we point the camera to the base and start moving the end-effector, keeping the reference point in the camera frame. The tracking module will output \mathbf{P}^I . Next, with recorded Θ and forward kinematics, we know the transformation from the robot base to the local frame of the end-effector \mathbf{T}_i^{EB} at each frame i . The coordinate of the reference point in the end-effector’s local frame is given by $\hat{P}_i^E = \mathbf{T}_i^{EB} \hat{P}_{ref}^B$, where \hat{P} denotes the homogeneous representation of P . Now that we have the keypoints on the image plane \mathbf{P}^I and their corresponding points in the end-effector frame \mathbf{P}^E , we can again use PnP to solve \mathbf{T}^{CE} .

IV. EXPERIMENT

We evaluate our proposed method in a simulation environment and on public real-world datasets. The accuracy of keypoint tracking and hand-eye calibration are analyzed. We compare our method with DREAM [7], EasyHeC [9] and the traditional marker-based method which is implemented in the `easy_handeye` software package.

A. Experimental Setup

1) *Evaluation in the simulation environment:* The simulation environment is built with the RFUniverse [15] simulator. The Franka Emika robot is placed on the ground. In the eye-on-base setting, a virtual camera is randomly placed and pointed at the robot. We record 20 video segments, each

lasting 10 seconds. Within each segment, the end-effector of the robot moves towards one random direction for 1s and then switches to another new random direction, repeating this cycle 10 times. The position of the end-effector target is also recorded to provide the ground truth for the keypoint tracking module. In the eye-in-hand setting, the virtual camera is attached to the end-effector. The robot’s movement is also random but under the constraint that the robot base is within the camera view. We configure the camera with a resolution of 1920×1080 , a field of view (FOV) of 60 degrees, and a frame rate of 30 Hz, aligning with real-world cameras in general. We compare the tracking and calibration results with the ground truth.

2) *Evaluation on the Real-World Dataset:* To evaluate the proposed method with real-world data, we resort to the DROID [16] dataset, a large, diverse, high-quality dataset for robot manipulation in the wild. It contains 1.7 TB of data from 564 different scenes, in each of which a Franka Emika Panda robot is mounted on a mobile platform with two eye-on-base cameras. The dataset provides RGB images and camera calibration matrices resulting from the traditional checkerboard-based calibration [36]. To note, since the dataset is too large, we select a subset of 60 video segments to test our proposed method. The selected video list will be made public.

In terms of calibration, since there is no ground truth available in the real world, we can use the reprojection error as an indirect indicator of the calibration accuracy. To be exact, we draw the mask of the Franka robot onto the camera frame based on the camera extrinsic produced by different methods and calculate the Intersection over Union (IoU) of the projected mask with the manually labeled ground truth masks on the first frame of each video. The higher IoU suggests a lower reprojection error and better accuracy.

B. Results on Keypoint Tracking

We first evaluate the zero-shot ability of the tracking module in the simulation environment. Given the 2D position of the TCP on the first frame, the tracking module keeps tracking its 2D position in the following frames. We measure the error between the predicted keypoint position and the ground truth. In Figure 4, we show the box plot of the error on x and y axes over the number of frames. The error quickly converges within ± 10 pixels. It shows no sign of divergence over the 300 frames, which indicates the tracking module powered by the visual foundation models is capable of accurately tracking the position of the TCP in the hand-eye calibration process.

C. Results on Hand-Eye Calibration

1) *Evaluation in simulation environment:* We test our hand-eye calibration pipeline in the simulation environment. In Table II, we report the results of our method and the traditional method in both eye-in-hand and eye-on-base settings. We compare with EasyHeC [9] and DREAM [7] in the eye-on-base setting only because they are not designed for eye-in-hand calibration. The proposed method achieves

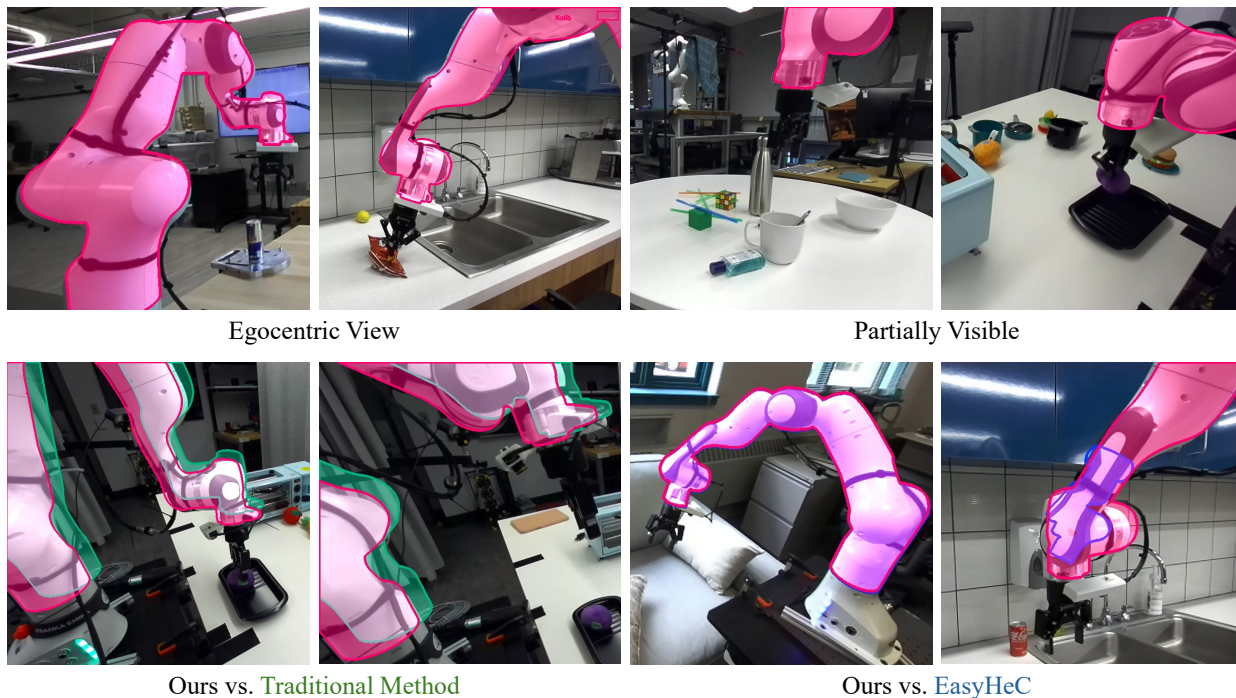


Fig. 3. Qualitative results. In the first row, we show the masks of the robot projected onto the camera frame with our method in red. In the second row, we compare our method with the traditional method on the left and with EasyHeC on the right. The green masks are from the traditional method, and the blue ones are from EasyHeC.

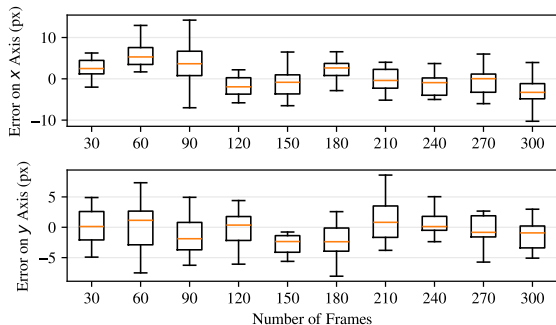


Fig. 4. Error of tracking over the number of frames in simulation.

TABLE II
CALIBRATION RESULTS IN SIMULATION

Setting	Method	e_x (cm)	e_y (cm)	e_z (cm)	e_r (deg)
EiH	Traditional	-0.21	0.20	1.44	0.78
	Ours	0.10	0.17	-0.21	0.69
EoB	Traditional	-0.21	0.55	3.19	1.00
	DREAM	0.64	1.02	6.36	4.84
	EasyHeC	1.14	-0.26	4.70	4.60
	Ours	-0.05	0.12	0.22	0.44

EiH stands for eye-in-hand, and EoB stands for eye-on-base. e_x , e_y , and e_z represent the averaged translational error on x , y , and z axis. e_r represents the averaged rotational error.

significantly better precision than the baseline methods. The traditional method produces larger error on z axis than x and y axes because of the nature of fiducial markers. We find EasyHeC may struggle when the robot is self-occluded or partially visible within the frame, which indicates some internal defects of its render-based optimization process. In comparison, the proposed method performs stably as long as the TCP is visible.

In terms of time consumption, the tracking module can run at ~ 5 frames per second (FPS) with a single RTX 3090 GPU, and therefore, each calibration process lasts around 2 minutes. EasyHeC, however, takes around 15 minutes for each calibration due to the relatively slow optimization speed of the differentiable renderer module. Plus, EasyHeC requires several extra hours to generate the Panda robot dataset in order to train the neural networks, while the proposed method can work out of the box.

2) *Evaluation on Real-World Dataset*: Recall that we use IoU between the manually-labeled mask and the reprojected mask to indirectly measure the calibration precision since there is no *ground truth* available in the real-world dataset. A higher IoU indicates a better calibration. On our test set, the proposed method achieves an average of 0.80 IoU. EasyHeC achieves 0.77 while the traditional, marker-based method achieves 0.87. The proposed method outperforms the baseline method but still has a slight gap to the marker-based method. The main reason behind this is that the DROID dataset is built for manipulation instead of calibration, and therefore, the pose and trajectory of the robot in the video segments are not optimized for calibration. Moreover, even

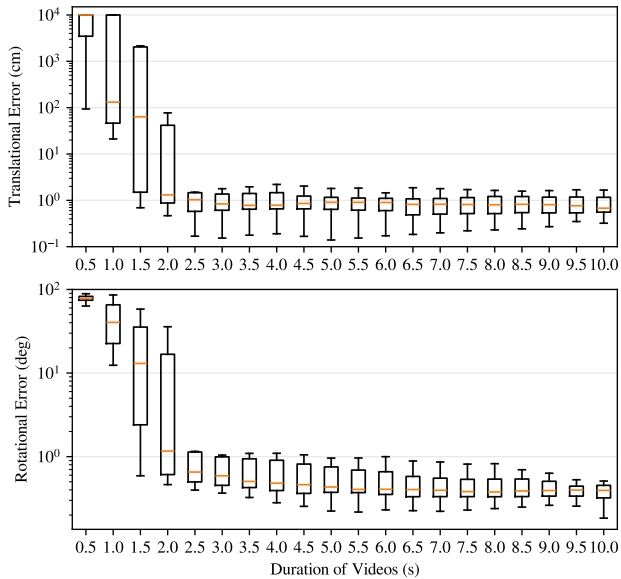


Fig. 5. Translational and rotational error over the duration of the video.

though the traditional method achieves the best averaged IoU, it's still far from ideal, confirming that the traditional methods can indeed fail in real-world applications, even in those expert-made datasets. Figure 3 shows a case of bad calibration from the dataset, and, in this case, the markerless methods can be applied as a post-hoc remedy to minimize the impact of the failure of calibration.

D. Ablation Studies

1) *Video Duration*: We analyse the effect of the video duration (*i.e.*, number of frames) on the calibration precision in the simulation environment. Figure 5 shows averaged translational and rotational error over the duration of the video. The error quickly converges below 1 cm or 1 degree after 3.0 seconds, indicating a 3-second video segment recording the robot's transforming between 3 poses is good for calibration. In practice, since the tracking process is automatic, we recommend moving the robot arm for several seconds longer and making the robot move to around 10 different poses, which can help make the calibration precise and robust to the possible noises.

2) *Choice of the Keypoint*: In theory, we can select multiple keypoints on the robot, since the tracking module can track an arbitrary number of keypoints simultaneously. However, as is discussed in Section III-B, not all joints are suitable candidates for keypoint tracking. We analyze the distance error of tracking different keypoints over 300 frames in the simulation environment. In Figure 6, we can find that the TCP achieves the lowest and the most stable tracking error, which proves the TCP is the best tracking candidate.

3) *Sensitivity Analysis*: We analyze the sensitivity of the PnP module. In the simulation environment, we first use the PnP module to estimate the transformation between ground truth 2D keypoints \mathbf{P}_{gt}^I and their 3D coordinates \mathbf{P}_{gt}^B . The accuracy of the resulting \mathbf{T}_{upper}^{CB} should be considered as the

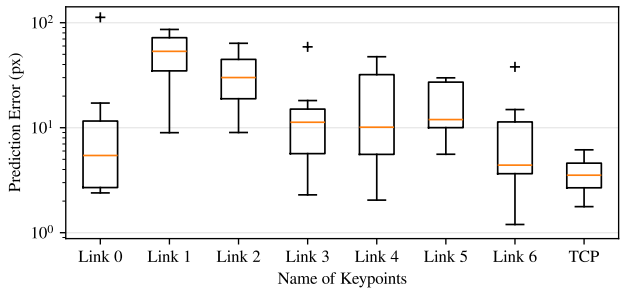


Fig. 6. Prediction error in Euclidean distance of different keypoint candidates, among which the TCP achieves the lowest and the most stable tracking error. Note that the y axis is on a log scale.

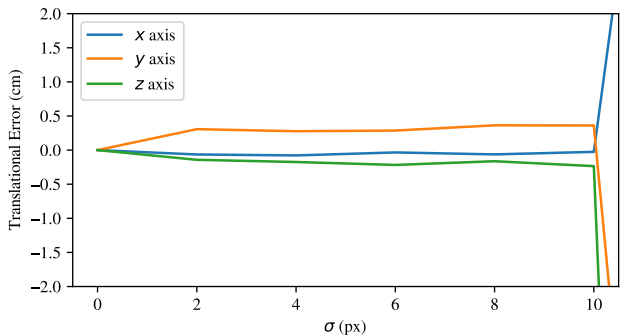


Fig. 7. Sensitivity analysis. The translational error increases with a larger noise.

upper bound of the proposed method. We then add random Gaussian noise $G(\mu, \sigma)$ to \mathbf{P}_{gt}^I , deriving \mathbf{P}^I . The resulting \mathbf{T}' will be impacted by the noise. We set $\mu = 0$, and $\sigma = 2, 4, 6, \dots$ to see how the accuracy is impacted by the noise. In Figure 7, we can see that the averaged error is below 1 cm when $\sigma \leq 10$ px. Considering the averaged distance error of tracking stays within several pixels in Figure 4, we can conclude that the PnP algorithm can handle the noise from the tracking module in our setting.

V. CONCLUSIONS, LIMITATIONS, AND DISCUSSION

In this letter, we present **Kalib**, an automatic markerless hand-eye calibration pipeline leveraging the visual foundation models for keypoint tracking. Kalib boasts its adaptability to new setups without training any neural networks. Also, there is no need for a calibration board or the robot's exact 3D mesh model. Results show that the proposed method outperforms the baseline methods and highlights its potential to be integrated into real-world scenarios like dataset construction.

However, the proposed method still suffers from the defects of common vision-based systems. For example, the tracking module may lose track when the background is too noisy, the reference point to track is too small, or motion blur occurs due to low ambient light. Future work can focus on improving the precision and generalizability of the whole pipeline. For example, the proposed method can immediately benefit from the future advancement of keypoint tracking to perform better under the aforementioned tricky conditions.

REFERENCES

- [1] F. Park and B. Martin, "Robot sensor calibration: solving $AX=XB$ on the Euclidean group," *IEEE Transactions on Robotics and Automation*, vol. 10, no. 5, pp. 717–721, Oct. 1994, conference Name: IEEE Transactions on Robotics and Automation. [Online]. Available: <https://ieeexplore.ieee.org/document/326576>
- [2] R. Horaud and F. Dornaika, "Hand-Eye Calibration," *The International Journal of Robotics Research*, vol. 14, no. 3, pp. 195–210, June 1995, publisher: SAGE Publications Ltd STM. [Online]. Available: <https://doi.org/10.1177/027836499501400301>
- [3] R. Tsai and R. Lenz, "A new technique for fully autonomous and efficient 3d robotics hand/eye calibration," *IEEE Transactions on Robotics and Automation*, vol. 5, no. 3, pp. 345–358, 1989.
- [4] M. Antonello, A. Gobbi, S. Michieletto, S. Ghidoni, and E. Menegatti, "A fully automatic hand-eye calibration system," in *2017 European Conference on Mobile Robots (ECMR)*. Paris: IEEE, Sept. 2017, pp. 1–6. [Online]. Available: <http://ieeexplore.ieee.org/document/8098681/>
- [5] E. Olson, "Apriltag: A robust and flexible visual fiducial system," in *ICRA*. IEEE, 2011, pp. 3400–3407. [Online]. Available: <http://dblp.uni-trier.de/db/conf/icra/icra2011.html#Olson11>
- [6] S. Garrido-Jurado, R. Muñoz-Salinas, F. J. Madrid-Cuevas, and M. J. Marín-Jiménez, "Automatic generation and detection of highly reliable fiducial markers under occlusion," *Pattern Recognition*, vol. 47, no. 6, pp. 2280–2292, 2014. [Online]. Available: <https://www.sciencedirect.com/science/article/pii/S0031320314000235>
- [7] T. E. Lee, J. Tremblay, T. To, J. Cheng, T. Mosier, O. Kroemer, D. Fox, and S. Birchfield, "Camera-to-robot pose estimation from a single image," in *2020 IEEE International Conference on Robotics and Automation (ICRA)*. IEEE, May 2020. [Online]. Available: <http://dx.doi.org/10.1109/ICRA40945.2020.9196596>
- [8] J. Lu, F. Richter, and M. C. Yip, "Markerless Camera-to-Robot Pose Estimation via Self-Supervised Sim-to-Real Transfer," in *2023 IEEE/CVF Conference on Computer Vision and Pattern Recognition (CVPR)*. Vancouver, BC, Canada: IEEE, June 2023, pp. 21 296–21 306. [Online]. Available: <https://ieeexplore.ieee.org/document/10204830/>
- [9] L. Chen, Y. Qin, X. Zhou, and H. Su, "Easyhec: Accurate and automatic hand-eye calibration via differentiable rendering and space exploration," *IEEE Robotics and Automation Letters*, vol. 8, no. 11, p. 7234–7241, Nov. 2023. [Online]. Available: <http://dx.doi.org/10.1109/LRA.2023.3315551>
- [10] B. C. Sefercik and B. Akgun, "Learning Markerless Robot-Depth Camera Calibration and End-Effector Pose Estimation," in *Conference on Robot Learning*, Aug. 2022. [Online]. Available: <https://openreview.net/forum?id=e18CZ2s267o>
- [11] J. Heller, M. Havlena, A. Sugimoto, and T. Pajdla, "Structure-from-motion based hand-eye calibration using $L_{S,8S}$ minimization," in *Proceedings of the 2011 IEEE Conference on Computer Vision and Pattern Recognition*, ser. CVPR '11. USA: IEEE Computer Society, June 2011, pp. 3497–3503. [Online]. Available: <https://doi.org/10.1109/CVPR.2011.5995629>
- [12] A. Kirillov, E. Mintun, N. Ravi, H. Mao, C. Rolland, L. Gustafson, T. Xiao, S. Whitehead, A. C. Berg, W.-Y. Lo, P. Dollár, and R. Girshick, "Segment anything," *arXiv:2304.02643*, 2023.
- [13] T. Ren, S. Liu, A. Zeng, J. Lin, K. Li, H. Cao, J. Chen, X. Huang, Y. Chen, F. Yan, Z. Zeng, H. Zhang, F. Li, J. Yang, H. Li, Q. Jiang, and L. Zhang, "Grounded sam: Assembling open-world models for diverse visual tasks," 2024.
- [14] N. Karaev, I. Rocco, B. Graham, N. Neverova, A. Vedaldi, and C. Rupprecht, "Cotracker: It is better to track together," *arXiv:2307.07635*, 2023.
- [15] H. Fu, W. Xu, R. Ye, H. Xue, Z. Yu, T. Tang, Y. Li, W. Du, J. Zhang, and C. Lu, "Demonstrating RFUniverse: A Multiphysics Simulation Platform for Embodied AI," in *Proceedings of Robotics: Science and Systems*, Daegu, Republic of Korea, July 2023.
- [16] A. Khazatsky, K. Pertsch, S. Nair, A. Balakrishna, S. Dasari, S. Karamcheti, S. Nasiriany, M. K. Srirama, L. Y. Chen, K. Ellis, P. D. Fagan, J. Hejna, M. Itkina, M. Lepert, Y. J. Ma, P. T. Miller, J. Wu, S. Belkhal, S. Dass, H. Ha, A. Jain, A. Lee, Y. Lee, M. Memmel, S. Park, I. Radosavovic, K. Wang, A. Zhan, K. Black, C. Chi, K. B. Hatch, S. Lin, J. Lu, J. Mercat, A. Rehman, P. R. Sanketi, A. Sharma, C. Simpson, Q. Vuong, H. R. Walke, B. Wulfe, T. Xiao, J. H. Yang, A. Yavary, T. Z. Zhao, C. Agia, R. Baijal, M. G. Castro, D. Chen, Q. Chen, T. Chung, J. Drake, E. P. Foster, J. Gao, D. A. Herrera, M. Heo, K. Hsu, J. Hu, D. Jackson, C. Le, Y. Li, R. Lin, Z. Ma, A. Maddukuri, S. Mirchandani, D. Morton, T. K. Nguyen, A. O'Neill, R. Scalise, D. Seale, V. Son, S. Tian, E. Tran, A. E. Wang, Y. Wu, A. Xie, J. Yang, P. Yin, Y. Zhang, O. Bastani, G. Berseth, J. Bohg, K. Goldberg, A. Gupta, A. Gupta, D. Jayaraman, J. J. Lim, J. Malik, R. Martín-Martín, S. Ramamoorthy, D. Sadigh, S. Song, J. Wu, M. C. Yip, Y. Zhu, T. Kollar, S. Levine, and C. Finn, "DROID: A large-scale in-the-wild robot manipulation dataset," in *RSS 2024 Workshop: Data Generation for Robotics*, 2024. [Online]. Available: <https://openreview.net/forum?id=Ml2pTYLNLi>
- [17] J. Ilonen and V. Kyrki, "Robust robot-camera calibration," in *2011 15th International Conference on Advanced Robotics (ICAR)*, 2011, pp. 67–74.
- [18] K. Daniilidis, "Hand-eye calibration using dual quaternions," *The International Journal of Robotics Research*, vol. 18, no. 3, pp. 286–298, 1999. [Online]. Available: <https://doi.org/10.1177/02783649922066213>
- [19] M. Fiala, "Artag, a fiducial marker system using digital techniques," in *2005 IEEE Computer Society Conference on Computer Vision and Pattern Recognition (CVPR'05)*, vol. 2, 2005, pp. 590–596 vol. 2.
- [20] L. Yang, Q. Cao, M. Lin, H. Zhang, and Z. Ma, "Robotic hand-eye calibration with depth camera: A sphere model approach," in *2018 4th International Conference on Control, Automation and Robotics (ICCAR)*. IEEE, 2018, pp. 104–110.
- [21] N. Andreff, R. Horaud, and B. Espiau, "Robot Hand-Eye Calibration Using Structure-from-Motion," *The International Journal of Robotics Research*, vol. 20, no. 3, pp. 228–248, Mar. 2001, publisher: SAGE Publications Ltd STM. [Online]. Available: <https://doi.org/10.1177/02783640122067372>
- [22] X. Zhi and S. Schwertfeger, "Simultaneous hand-eye calibration and reconstruction," in *2017 IEEE/RSJ International Conference on Intelligent Robots and Systems (IROS)*, Sept. 2017, pp. 1470–1477, iSSN: 2153-0866. [Online]. Available: <https://ieeexplore.ieee.org/document/8205949>
- [23] E. Valassakis, K. Dreczkowski, and E. Johns, "Learning eye-in-hand camera calibration from a single image," in *Conference on Robot Learning*, 2021. [Online]. Available: <https://api.semanticscholar.org/CorpusID:240419785>
- [24] B. Wen, W. Yang, J. Kautz, and S. Birchfield, "Foundationpose: Unified 6d pose estimation and tracking of novel objects," in *Proceedings of the IEEE/CVF Conference on Computer Vision and Pattern Recognition (CVPR)*, June 2024, pp. 17 868–17 879.
- [25] M. Black and P. Anandan, "A framework for the robust estimation of optical flow," in *1993 (4th) International Conference on Computer Vision*, 1993, pp. 231–236.
- [26] B. D. Lucas and T. Kanade, "An iterative image registration technique with an application to stereo vision," in *Proceedings of the 7th International Joint Conference on Artificial Intelligence - Volume 2*, ser. IJCAI'81. San Francisco, CA, USA: Morgan Kaufmann Publishers Inc., 1981, p. 674–679.
- [27] M. Jaward, L. Mihaylova, N. Canagarajah, and D. Bull, "Multiple object tracking using particle filters," in *2006 IEEE Aerospace Conference*, 2006, p. 8.
- [28] M. Arulampalam, S. Maskell, N. Gordon, and T. Clapp, "A tutorial on particle filters for online nonlinear/non-gaussian bayesian tracking," *IEEE Transactions on Signal Processing*, vol. 50, no. 2, pp. 174–188, 2002.
- [29] C. Doersch, Y. Yang, M. Vecerik, D. Gokay, A. Gupta, Y. Aytar, J. Carreira, and A. Zisserman, "Tapir: Tracking any point with per-frame initialization and temporal refinement," in *2023 IEEE/CVF International Conference on Computer Vision (ICCV)*. IEEE, Oct. 2023. [Online]. Available: <http://dx.doi.org/10.1109/ICCV51070.2023.00923>
- [30] N. Tumanyan, A. Singer, S. Bagon, and T. Dekel, "Dino-tracker: Taming dino for self-supervised point tracking in a single video," March 2024.
- [31] Y. Xiao, Q. Wang, S. Zhang, N. Xue, S. Peng, Y. Shen, and X. Zhou, "Spatialtracker: Tracking any 2d pixels in 3d space," in *Proceedings of the IEEE/CVF Conference on Computer Vision and Pattern Recognition (CVPR)*, 2024.
- [32] J. Denavit and R. S. Hartenberg, "A Kinematic Notation for Lower-Pair Mechanisms Based on Matrices," *Journal of Applied Mechanics*, vol. 22, no. 2, pp. 215–221, June 1955. [Online]. Available: <https://doi.org/10.1115/1.4011045>
- [33] Long Quan and Zhongdan Lan, "Linear N-point camera pose determination," *IEEE Transactions on Pattern Analysis and Machine*

- Intelligence*, vol. 21, no. 8, pp. 774–780, Aug. 1999. [Online]. Available: <http://ieeexplore.ieee.org/document/784291/>
- [34] V. Lepetit, F. Moreno-Noguer, and P. Fua, “EPnP: An Accurate $O(n)$ Solution to the PnP Problem,” *International Journal of Computer Vision*, vol. 81, no. 2, pp. 155–166, Feb. 2009. [Online]. Available: <https://doi.org/10.1007/s11263-008-0152-6>
- [35] M. Zuliani, “Ransac for dummies,” Tech. Rep., Nov. 2008.
- [36] G. Bradski, “The OpenCV Library,” *Dr. Dobb’s Journal of Software Tools*, 2000.